*

A quasi-static controller of tendon-driven continuum robots based on analytical differential kinematics

Weiming Ba[1], Jung-Che Chang[1], Jing Liu[1], Xi Wang[1], Xin Dong*[1] and Dragos Axinte[1]

Abstract

Generic and high-performance feedback control is still challenging for tendon-driven continuum robots. Conventional model-based controllers, based on the piecewise constant curvature (PCC) assumption, explicitly require the arc parameters (bending angle and direction angle) to link the task (in Cartesian coordinates) and actuation spaces. However, the approaches' effectiveness remains to be explored when robot shapes deviate from circular arcs. This paper proposed a hybrid scheme for novel kinematic control of continuum robots. The error led by the slack state has been avoided through tension supervision, while analytical differential kinematics is further developed to avoid the explicit call of arc parameters by importing Cylindrical coordinates into task space and applying accurate piecewise linear approximation. Comparison between a conventional PCC-based controller and the proposed controller has been done by implementing them to a twin-pivot joint-based continuum section. An overall tip positioning accuracy of ±0.35mm has been reached, and a result of root-mean-square-error (RMSE): 0.3mm and Max error: 0.97mm has been observed when running two predefined path tracking. Further, in order to evaluate the versatility of the proposed controller, a dual-revolute joint-based and a 3D-printed continuum section were used to test for path tracking to prove the effectiveness of the controller on a wide range of continuum robotic systems.

Keywords: Continuum robot, tension supervision, differential kinematics

1 Introduction

Continuum robots outperform conventional rigid-link robots in terms of the ability to have access to confined environments owing to their compliant mechanical property achieved by various structural designs. It can be classified into two categories based on their actuation mechanism: intrinsic actuation and extrinsic actuation[1]. In extrinsically actuated continuum robots, the actuators are typically positioned at the base of the backbone. Examples of such robots include tendon-driven continuum robots and concentric tube continuum robots. Among them, tendon-driven continuum robots have been designed with various structures[2], such as flexible backbone [3], twin-pivot [4]/dual-revolute joint [5] and elastic flexible material [6]. Regarding intrinsically actuated continuum robots, their actuators are distributed along their backbone. This distribution allows for various actuation methods, including pneumatic, hydraulic, shape-memory alloy (SMA), electrical polymer actuation, and hygroscopic actuation[7]. Compared to hydraulic/pneumatic method, the tendon-driven approach has faster responding speed, and allows large length-diameter-ratio structural design, enabling more promising applications in confined environments, for example, minimally invasive surgery [3, 8, 9] and in-situ maintenance of aero-engines [4, 5].

Open-loop control and Close-loop control have both been developed for continuum robots. The former approach offers less dimensional limitations by freeing from the use of the integrated sensor. The significant reliance of the actuation accuracy to the model inversion bloomed the improvement of accurate modellings. Ref.

* Corresponding author: Xin Dong (Xin.Dong@nottingham.ac.uk).

[1] Weiming Ba, Jung-Che Chang, Jing Liu, Xi Wang, Xin Dong, and Dragos Axinte are with Faculty of Engineering, University of Nottingham, Nottingham NG8 1BB, UK.

[10] applied a reinforcement learning method with Markov Decision Process to learn open-loop control strategy from simulation on a 300mm-long pneumatic manipulator, achieving a mean error of 30.5mm for positioning. Having a clearer comparison to the conventional approach, ref. [11] proposed a feed-forward method employing neural network to learn the inverse statics of a 280mm-long soft robot. The experiments demonstrate that the learning method outperforms the model-based Jacobian approach in terms of positional accuracy (mean error of feedforward neural network (NN): 7.35mm; that of model-based Jacobian approach: 15.12mm). Overall, the implementation of machine learnings from both works shows necessity of dealing with the hard-to-predict factors such as potential frictions, dimensional errors, and actuation cable.

With respect to close-loop control of continuum robots, both model-based and model-less approaches have been developed. The model-based methods, also called quantitative approaches, are induced from the physical model of different robotic systems. Owing to the briefness and efficacy, the piecewise constant curvature (PCC) assumption [12-14] is still the most common kinematic model applied for the feedback control of continuum robots. As examples, optimal control was employed on a 170mm-long continuum robot with two extensible modules for smooth path tracking by minimizing the overall cable displacements [15], which can keep the maximum tracking error less than 3mm for a circular path. Orientation control is performed in [16] on a single-section pneumatic robot (4.9mm in diameter and 20mm in length) in joint space, achieving average errors of 0.01º and 0.4º in bending angle and direction angle, respectively. Also, the weighted Jacobian controller is realized in [17] by fuzzy-control rules on a 3 degree of freedoms (DoFs) cable-driven continuum manipulator (length: 143mm; maximum contraction rate: 30%) for spatial linear path tracking, achieving 0.72mm positioning accuracy at the end point. Performing the lumped parameter formulation to drive the dynamic model of a 2-DoF cable-driven soft manipulator (length: 80mm) with additional 1-DoF for linear insertion in [18], the maximum following error from 50mm (open-loop) to 18mm has been reduced at an average velocity of 16.7mm/s.

The model-less control of continuum and soft robots could be classified into two approaches: online learning and off-line learning. Based on online learning, [19] applied real-time Jacobian estimation on a planar cable-driven robot (length: 280mm) with linear feed-in mechanism, which reaches 1.22±0.93mm accuracy tracking a square trajectory in free space. However, this work takes the assumption that tendon tensions are proportional to tendon displacements, which neglects the disturbances of frictions and hence restricts its further application on other cable-driven robotic systems. Similar method is implemented in [20] on a novel 5-section pneumatic manipulator with each section constructed by four groups of inflatable airbags, realizing 5mm accuracy for point-to-point motion at 1 Hz feedback frequency. Another case is shown in [21], which uses locally weighted projection regression to learn the global controller from multiple controllers in local regions for orientation control of a 2-DoF pneumatic soft manipulator (length: 93mm), achieving ±4.24º maximum absolute error in first cycle and ±1.92º after several cycles. Additionally, Kalman filter is also applied for Jacobian estimation to deal with system uncertainty and external disturbances (by assuming process and measurement noise as white Gaussian noise) on a 2-section extensible pneumatic manipulator (original full length: 400mm) in [22], which can reach 2.31mm average root-mean-square-error (RMSE) when tracking a circular path.

Off-line learning, especially neural network (NN), is a more widely used approach for the continuum robot. In [23], adaptive neural network control is realized on compact bionic handling assistant, a 2-section inextensible pneumatic manipulator (length: 360mm). The controller consists of two sub-controllers: the distal supervised learning controller is for forward and inverse kinematic models offline training while the adaptive controller is designed to learn controller by multilayer perceptron and emulator by modified Elman neural network and reaches ±5mm average error for path tracking. Also, an example is given in [24] where neural network is utilized on a 2-section inextensible cable-driven continuum robot (length: 405mm) and the learnt model is integrated into the feedback control, realizing 9.67mm mean error for point-to-point motion and 23mm average error for line following. Overall, for those model-based methods, they are developed on explicit models and thus can be analysed theoretically and modified for different tasks; however, they cannot deal with the uncertainty and nonlinearity of continuum robots, so that the model uncertainties/errors are usually difficult to compensate for [11, 25]. In terms of model-less methods, the control policies are usually learnt from massive data or developed based on other algorithms, which can be directly deployed on different continuum robots, but their unclear working mechanism makes it difficult for further optimisation and unsuitable for dynamic control especially under external disturbances[26].

Aiming to combine the advantages of both model-based and model-less approaches, a generic controller was developed in this paper. By describing the tip position using Cylindrical coordinates and applying piecewise linear fitting, a novel analytical differential kinematics directly from task space to actuation space was derived based on the conventional PCC model, which avoids the explicit call of arc parameters (bending angle θ and direction angle φ). On the other hand, after the analysis of control schemes of tendon-driven continuum robots,

tension supervision was integrated into the controller design by setting a threshold value to the cable tension to eliminate cables from being slack, which decouples the cable control and avoids the backlash in robot operation. As a comparison, the proposed and PCC-based hybrid controllers are both implemented on the twin-pivot design [27] for tip positioning and path tracking. Then, the proposed controller is further implemented on a dual-revolute joint based continuum section and a 3D-printed based continuum section to prove the versatility of the proposed controller.

The rest of the paper is organized as follows. Chapter II proposes the innovative hybrid control scheme and presents the formulation of the novel differential kinematics. Then, test-rig setup and experimental results on different prototypes are given in Chapter III. Finally, Chapter IV goes to the conclusion and further discussion.

2 Control Methodology

In this section, a model-based controller is developed, which can avoid the explicit call of arc parameters and keeps the analytical form directly from task (desired position) to actuation space (cable displacement). Further, the proposed controller is integrated with tension supervision to keep all driving cables in tension, thus avoiding the robot backlash.

2.1 Analysis of different control schemes

In general, the controller design of tendon-driven continuum robots is mostly based on cable displacements (Fig. 1 (a)), which are the only variables controlled directly at the hardware level. This control mode is used in most of the research for close-loop control of continuum robots as it is easy to implement and control. Besides, considering that the shape deformation of continuum robots is essentially the result of the interactions between the robots and driving cables, an alternative control mode of continuum robots is by cable tensions (Fig. 1(b)). However, this mode is hardly applied in feedback control owing to the great challenge of designing controllers for the robot shape (tip position/orientation) and cable tensions, especially for multi-section continuum robots where complex mechanics interactions exist between sections and cables.

Regarding single-section continuum robots, the tension loss of driving cables is negligible. As such, the actual cable tensions can be measured relatively accurately with load cells at the actuation end. Therefore, cable tensions can also be utilized to design controllers for single-section continuum robots. An example is given in Fig. 1(c) to illustrate the schematic diagram of hybrid control. For the robot configuration indicated in the figure, the red cable dominates the section's bending motion, while the other two cables (green and blue) are responsible for the circumferential motion. However, it is obvious that there is no need to control the green and blue cables simultaneously for circumferential motion. The section motion can be fully operated with two active cables at any moment, with the third passive cable in a proper tension to keep the robot structure compact. With such a control scheme, the displacements of three driving cables can be decoupled in a kinematic level. More importantly, by importing the tension supervision, ill cables states, such as over-tension or slack, can be avoided.

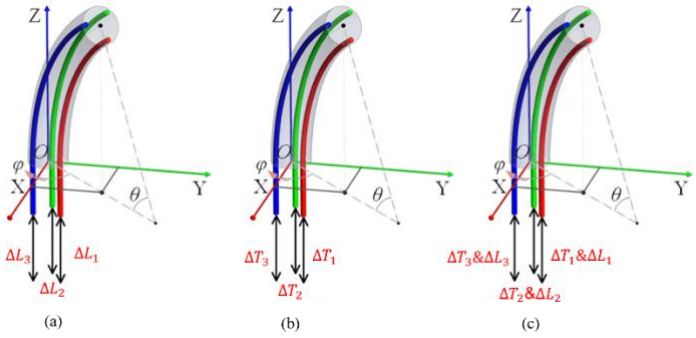

Fig. 1 Different control modes for tendon-driven continuum robots: (a) by cable displacements (ΔL_1, ΔL_2, ΔL_3); (b) by cable tensions (ΔT_1, ΔT_2, ΔT_3); (c) combination of cable displacements and tensions ($\Delta L_1 \& \Delta T_1$, $\Delta L_2 \& \Delta T_2$, $\Delta L_3 \& \Delta T_3$).

2.2 Formulation of the novel differential kinematics

The classical kinematic model is shown in Fig. 2(a), which consists of three levels in hierarchy, namely, actuation space(L_1, L_2, L_3), configuration space(θ, φ) and task space(x, y, z). Configuration space is the bridge to build the mapping between actuation and task space with a constant-curvature assumption. This kinematic model provides a brief and effective way to describe and model the shape of continuum robots, based on which, different model-based close-loop controllers are designed and validated on various prototypes of continuum robots. However, this model introduced two additional variables which are actually unmeasurable intermediates. This method would lead to singularity when the continuum section is in a zero bending angle. Also, it requires an inverse calculation to the constructed Jacobian matrix.

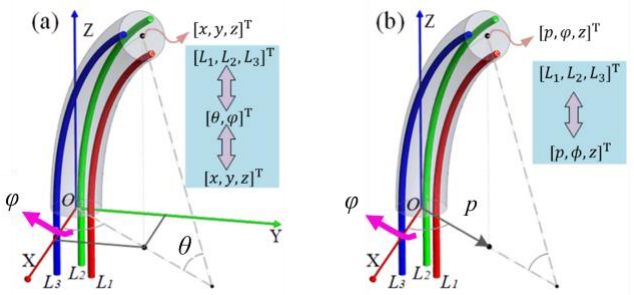

Fig. 2 Schematic of (a) the conventional PCC-based kinematic model and (b) the modified kinematic model.

Based on the above discussion, a modified kinematic model is proposed in this section to address the above-mentioned challenges of the conventional model. As shown in Fig. 2(b), the tip position is described with Cylindrical coordinates (p, ϕ, z) instead of Cartesian coordinates (x, y, z) in Fig. 2(a). Further, since single section of inextensible continuum robots have only 2-DoF, the variables (p, ϕ, z) in task space are not totally independent from each other. Once (p, ϕ) is chosen, the value of z is determined, even though the explicit expression of the function $z = f(p, \phi)$ is unknown. Hence, the parameter pair of (p, ϕ) is necessary and sufficient for the derivation of the modified kinematic model.

Based on the constant-curvature assumption, the kinematics from configuration to task space can be written as:

$$\begin{bmatrix} p \\ \phi \end{bmatrix} = \begin{bmatrix} S \cdot \dfrac{1-\cos\theta}{\theta} \\ \varphi \end{bmatrix} \tag{1}$$

where S denotes the backbone length of the continuum robot.

The red curve in Fig. 3(a) is the function of $f(\theta) = \frac{1-\cos\theta}{\theta}\left(\theta \in \left[0, \frac{\pi}{2}\right]\right)$, which is nonlinear but highly positively related to θ. Thus, a linear fitting approach is considered to linearize $f(\theta)$ for the following derivation. To reach low deviation ratio $e(\theta) = max\left(\left|\frac{f(\theta)-l(\theta)}{f(\theta)}\right|, \forall\theta \in \left[0, \frac{\pi}{2}\right]\right)$, a piece-wise line with three segments is adopted for the curve fitting. The whole variation range of θ is divided into three subsets: $U_1 = [0, \frac{\pi}{6}), U_2 = [\frac{\pi}{6}, \frac{\pi}{3}), U_3 = [\frac{\pi}{3}, \frac{\pi}{2}]$. In each subset, $f(\theta)$ is approximated by single segment whose endpoints overlap with those of $f(\theta)$. Fig. 3(b) gives the deviation ratio in the full range, of which the maximum deviation ratio (2.26%) is below 2.5%. Obviously, the maximum deviation ratio can be further reduced by dividing the range of θ into more subsets. However, considering the balance of simplicity and accuracy, the division using three segmented lines is finally adopted.

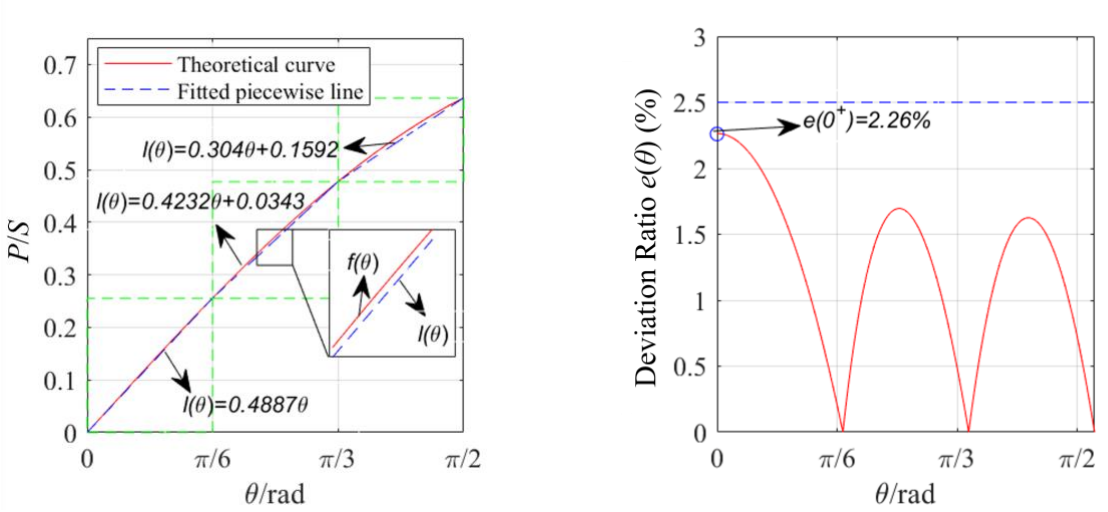

(a) (b)

Fig. 3 Curve fitting of the function $f(\theta)=\frac{p}{s}=\frac{1-cos\,\theta}{\theta}$: (a) $f(\theta)$ is approximated by three segmented lines $l(\theta)$; (b) fitting error with respect to bending angle $\in[0,\frac{\pi}{2}]$

Thus, $f(\theta)$ can be linearized with high accuracy as below:

$$f(\theta)=k_j\theta+b_j,\theta\in U_j(j=1,2,3) \tag{2}$$

where $\begin{bmatrix}k_1 & b_1\\ k_2 & b_2\\ k_3 & b_3\end{bmatrix}=\begin{bmatrix}0.4887 & 0\\ 0.4232 & 0.0343\\ 0.304 & 0.1592\end{bmatrix}$.

Combining (1) and (2), the expression of the radial coordinate p can be rewritten as:

$$p=S\cdot(k_j\theta+b_j),\theta\in U_j(j=1,2,3) \tag{3}$$

Hence, the derivative of p with respect to the bending angle θ can be obtained:

$$\frac{dp}{d\theta}=Sk_j,\theta\in U_j(j=1,2,3) \tag{4}$$

Eq. (5) gives the kinematics from configuration space (θ,φ) to cable displacements in actuation space (L_1,L_2,L_3):

$$\begin{bmatrix}L_1\\ L_2\\ L_3\end{bmatrix}=S-r\theta\cdot\begin{bmatrix}\cos(\alpha_1-\varphi)\\ \cos(\alpha_2-\varphi)\\ \cos(\alpha_3-\varphi)\end{bmatrix} \tag{5}$$

where r denotes the radius of circle on which all the driving cables are distributed while $\alpha_1,\alpha_2,\alpha_3$ are the phase angles with respect to X axis in the XY plane indicating the location of each cable.

Since continuum robots are usually initialized to be straight, the initial values of L_1, L_2 and L_3 are all equal to S. Therefore, the increment of all the cables within the continuum robot can be written as below:

$$\begin{bmatrix}\delta L_1\\ \delta L_2\\ \delta L_3\end{bmatrix}=\begin{bmatrix}L_1\\ L_2\\ L_3\end{bmatrix}-S \tag{6}$$

Putting (5) into (6), we can get:

$$\begin{bmatrix}\delta L_1\\ \delta L_2\\ \delta L_3\end{bmatrix}=-r\theta\cdot\begin{bmatrix}\cos(\alpha_1-\varphi)\\ \cos(\alpha_2-\varphi)\\ \cos(\alpha_3-\varphi)\end{bmatrix} \tag{7}$$

Then, we can start to derive the differential kinematics from task space (p,φ) to actuation space (L_1,L_2,L_3), based on which the feedback controller is designed. The derivative of the cable displacement changes $d\delta L_i$ with respect to the Cylindrical coordinates p and ϕ can be written as below:

$$d\delta L_i=\frac{\partial\delta L_i}{\partial p}\cdot dp+\frac{\partial\delta L_i}{\partial\phi}\cdot d\phi,i=1,2,3 \tag{8}$$

According to the chain rule for derivative and (4), the first coefficient on the right side of (8) can be computed as:

$$\frac{\partial \delta L_i}{\partial p} = \frac{\partial \delta L_i}{\partial \theta} \Big/ \frac{dp}{d\theta} = -\frac{r}{Sk_j} \cdot \cos(\alpha_i - \phi),\ j = 1, 2, 3 \tag{9}$$

It should be noticed that θ is not explicitly called in (9), which is achieved by the linearization of p in (3). The interval mapping relationship of θ and p is given below:

$$U_1 = [0, \frac{\pi}{6}) \leftrightarrow \Omega_1 = S \cdot [0, 0.2559)$$
$$U_2 = [\frac{\pi}{6}, \frac{\pi}{3}) \leftrightarrow \Omega_2 = S \cdot [0.2559, 0.4775)$$
$$U_3 = [\frac{\pi}{3}, \frac{\pi}{2}] \leftrightarrow \Omega_3 = S \cdot [0.4775, 0.6366]$$

There, we obtain the explicit expression of the differential kinematics directly from task space to actuation space:

$$d\delta L_i = \frac{r}{k_j} \cdot \left[-\frac{\cos(\alpha_i - \phi)}{S} \cdot dp + (\frac{p}{S} - b_j) \cdot \sin(\alpha_i - \phi) \cdot d\phi \right] \tag{10}$$

Here, it can be found that a direct mapping between actuation and task space is established, while the bending and direction angles are not involved.

Further, since Cartesian coordinate system is more intuitive and commonly used for both input and feedback, the following transformations are necessary for algorithm implementation:

$$\begin{cases} p = \sqrt{x_d^2 + y_d^2} \\ \phi = atan2(y_d, x_d) \\ dp = \sqrt{x_a^2 + y_a^2} - \sqrt{x_d^2 + y_d^2} \\ d\phi = atan2(y_a, x_a) - atan2(y_d, x_d) \end{cases} \tag{11}$$

where (x_d, y_d) denotes the desired tip position while (x_a, y_a) is the actual tip position.

Therefore, the inverse kinematic model could be obtained by substituting eq (11) for eq (10). In the experiments, the actual tip position (x_a, y_a) are measured by a vision-based tracking system as a feedback of the controller, while the bending angle θ is not used.

In addition, since the angular coordinate $\phi \in (-\pi, \pi]$, the domain of $d\varphi$ becomes discontinuous for quadrant switch between quadrant 2 and quadrant 4, which can be solved by the rules shown below:

$$d\phi < -\pi, d\phi + 2\pi \rightarrow d\phi$$
$$d\phi > \pi, d\phi - 2\pi \rightarrow d\phi$$

By utilizing the derived model, the motion control of the continuum robot (p and φ) can be decoupled and linearized by controlling the variations of the three cables (L_1, L_2 and L_3). Therefore, the sign (positive or negative) of the control inputs can be correctly obtained from this model, ensuring the closed loop system to be always stable.

2.3 Construction of the hybrid feedback controller

In the previous sub-section, the differential kinematics directly from task space (p, ϕ) to actuation space (L_1, L_2, L_3) was derived, based on which a universal controller for various arc-like tendon driven continuum robots can be developed. However, the slack state of driving cables is still inevitable as the errors accumulate owing to the factors like robot shape deviation, cable elongation caused by friction etc., which can result in backlash during robot manipulation. To solve the problem, tension supervision is integrated into the developed controller to keep all the driving cables in tension. It is worth mentioning that maintaining a certain cable with a constant tension cannot be achieved for the control of continuum robots since the state switching between active/passive cables in Section II.A occurs to all three cables when the robot moves in the whole workspace and the movement direction of the section tip varies. Instead, a lower limit τ is set to the tensions T_i of all the cables to prevent them from being slack, which can be expressed in the form of pseudo-code:

$$if\,(T_i \leq \tau\ \&\ d\delta L_i > 0), then\ d\delta L_i = 0\ (i = 1,2,3).$$

where the setting of the tension threshold is to select the largest possible value after considering the friction between the cable and vertebrae and the design of the robot.

For comparison, the proposed controller, as well as the PCC-based approach are both implemented with the tension supervision integrated. Fig. 4(a) shows the control diagram of the conventional PCC-based static controller [29]. As shown in the figure, the desired cable length L_d and actual cable length L_a are computed utilizing the inverse kinematics from the task space to the configuration space ("T.S-C.S IK") and from the configuration space to the actuation space ("C.S-A.S IK"), whose difference ΔL will then be multiplied by the gain coefficient $K(\in (0,1])$ and be regulated by the tension supervision block. In aspect to the proposed controller in Fig. 4(b), the target position (x_d, y_d) and the actual position (x_a, y_a) are firstly converted to (p_d, φ_d) and (p_a, φ_a) from the Cartesian coordinates to the Cylindrical coordinates. Then the desired position (p_d, φ_d) and position error $(\Delta p, \Delta \varphi)$ are used as the input of the modified differential inverse kinematics directly from the task space to the actuation space ("T.S-A.S Differential IK"), whose output, the cable displacements ΔL, will be multiplied by the gain coefficient $\eta(\in (0,1])$ and be regulated by the tension supervision block.

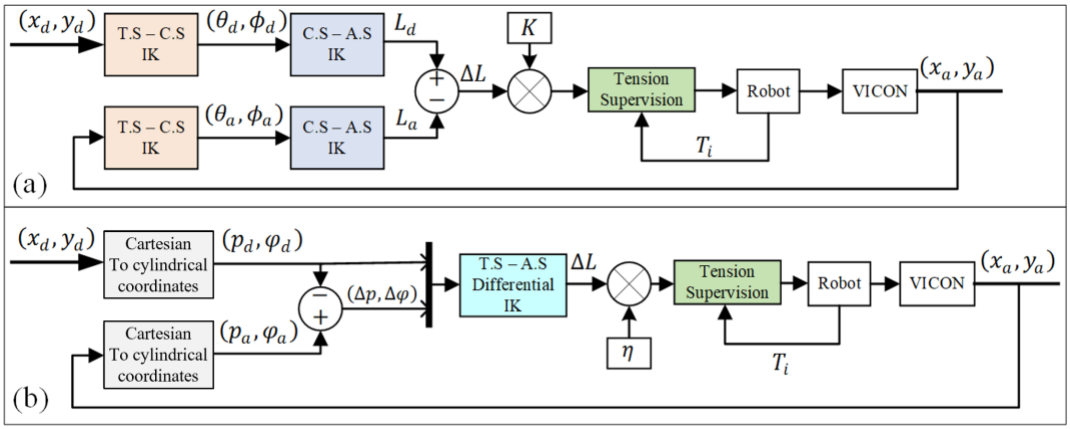

Fig. 4 Control architectures of (a) the PCC-based static controller and (b) the proposed controller. In the PCC-based controller, the arc parameters in configuration space are used as a transition to perform the differential inverse kinematics from task space to actuation space, while in the proposed controller, the target tip position is converted from Cartesian coordinates to cylindrical coordinates, with which the direct inverse kinematics is implemented without the explicit call of arc parameters. Additionally, tension supervision is integrated into both controllers at the level of cable displacement control. Where the abbreviations where as follow: T.S.: task space, CS: configuration space, AS: actuation space, and IK: inverse kinemactics.

3 Experimental Validation

In this section, a series of experiments are conducted to validate the hybrid controllers developed in the previous section. The test-rig is first introduced, which will be used as the platform to test continuum robots with various designs. Then, for the purpose of comparison, both the PCC-based and proposed hybrid controllers are implemented on the twin-pivot design for tip positioning and path tracking. Further experiments are also conducted on the other two prototypes (dual-revolute design and soft robot) to prove the versatility of the proposed controller.

3.1 Test-rig Setup

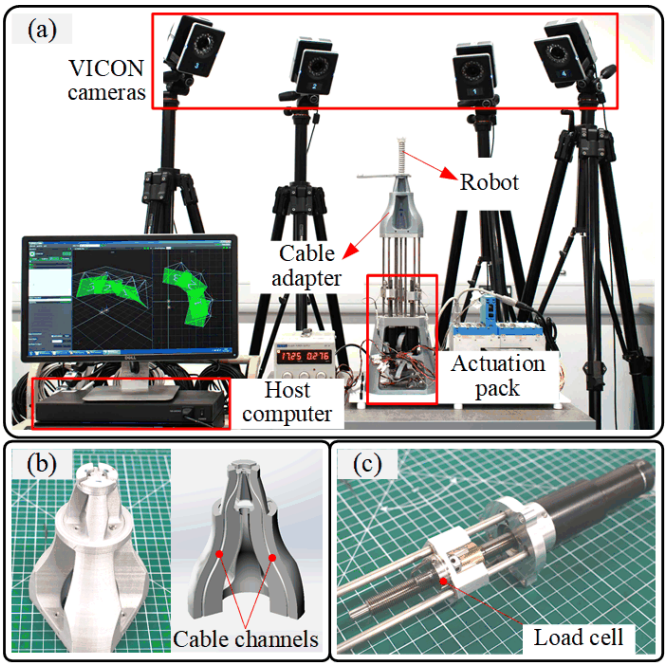

Fig. 5 (a) Test-rig setup, (b) 3D-printed cable adapter and (c) single motor module.

The whole test-rig is shown in Fig. 5(a), which consists of a host controller, a visual feedback device and an actuation pack. The host controller is a 64-bit Windows 7 based computer with an Intel Xeon E5-1620 processor @3.5 GHz and 16 GB RAM, and the VICON system is deployed as the visual feedback device to track the tip position and stream data at the frequency of 100 Hz. The main control program runs the proposed controller and sends commands to the motor controllers for cable displacement control while the data acquisition program reads the data from VICON and computes the real-time tip position for the main program to read. Two traceable objects are set for Vicon to respectively capture the position of the continuum section tip and root. The object for the continuum section root has a 100mm horizontal offset to avoid the robot body blocking the capture of the object. The mentioned horizontal offset and the vertical offset of the object for continuum tip, which caused by the thickness of the object base, have latterly been compensated for during the data processing.

The actuation system consists of a cable adapter (Fig. 5(b)) and three sets of motor modules (Fig. 5(c)). The adapter is 3D printed by PLA with three channels (ϕ4mm) inside to guide the driving cables (ϕ0.8mm includes the clear plastic protection tube) from the robot to the motor modules with negligible friction. Each motor module is made up of a Maxon DC motor, an EPOS2 50/5 position controller and a load cell (LCM201-200N). Two rods fixed on the stand pass through the slider on the motor shaft to prevent it from rotation so that the slider can only do linear motion along the shaft, which is precisely controlled by the motor controller. In addition, the load cell is taken as the intermediate between the slider and the driven cable, with one side mounted on the slider and the other side connected to the cable for tension measurement.

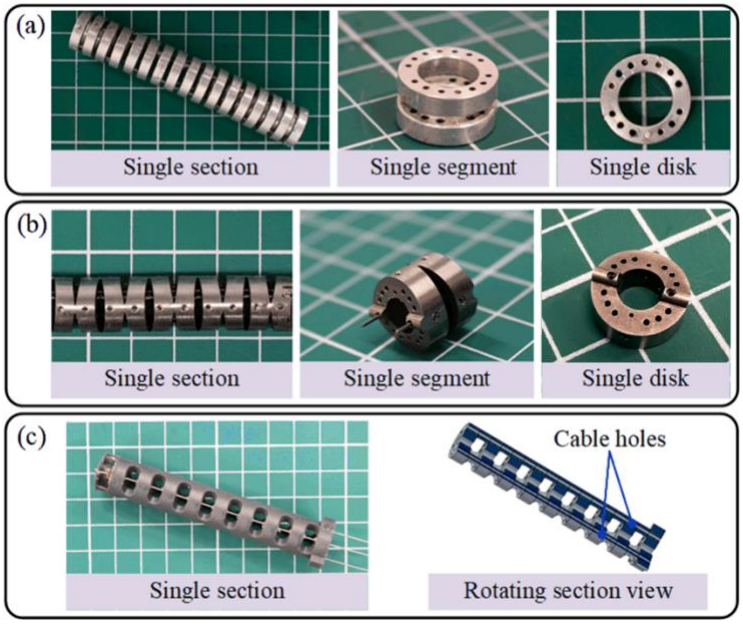

Fig. 6 Various prototypes of continuum robots for experiments: (a) twin-pivot design (2-DoF; length: 80mm; diameter: 15mm, cable hole size 1mm); (b) dual-revolute design (2-DoF; length: 55mm; diameter: 12.5mm, cable hole size 1mm), (c) soft robot by 3D printing (3-DoF; length: 80mm; diameter: 15mm, cable hole size 1mm).

The prototypes of single-section continuum robots utilized for experiments are shown in Fig. 6(a), and Fig. 6(b) illustrate the structure of the twin-pivot design in [4] and the dual-revolute design in [5], respectively. Both designs adopt NiTi rods for the connection between disks and to obtain compliant capability for bending motion. The soft-robot design is given in Fig. 6(c), which is 3D printed by resin and can be compressed along the length direction. The hybrid controllers are to be implemented on those designs for experimental validation.

3.2 Experiment I: tip positioning

a) Comparison of both controllers

The PCC-based method is widely accepted as a fundamental model-based approach in the entire field of continuum robotics, since it can represent the shape of continuum sections with minimal errors and computing time. Hence, the PCC-based method is usually selected as the baseline method to compare when new approaches are developed.

To achieve the optimal performance, the parameter tuning process is needed for the gain coefficients K in the PCC-based controller and η in the proposed controller before the comprehensive experiments. Comparing the response curves of positioning experiments under different controller parameters, 0.1 and 0.02 were taken as the best parameters through this comparative process.

Further comparisons of tip positioning were made between both controllers after the parameter tuning process. Eight sets of motions are chosen within the workspace for testing, among which the results of two tests (Fig.7 (a)) shows that both controllers perform well for the motion $(-30,35) \rightarrow (-35,35)$. However, when the motion comes to the boundary of the workspace ($(-35,35) \rightarrow (-40,40)$), oscillation occurs to the PCC-based controller while the proposed controller keeps steady with fast converging speed.

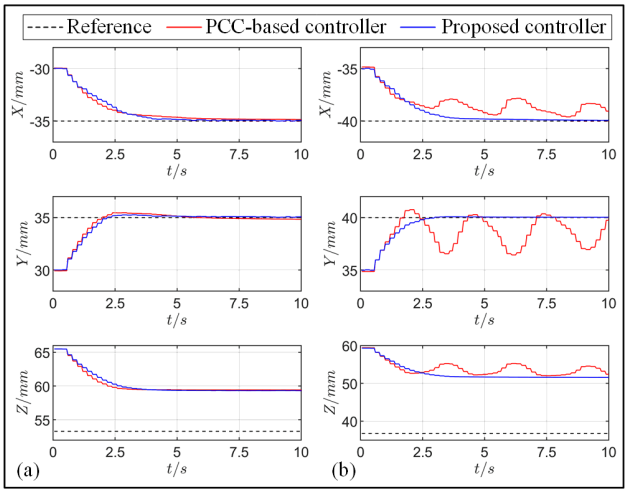

Fig. 7 Experimental comparison between the PCC-based and proposed hybrid controllers for tip positioning: (a) (−30,30)→(−35,35); (b) (−35,35)→(−40,40) (This set of experiments was taken by VICON system. The static error of the system is $\pm 0.15 \pm 0.025mm$ [30].)

Overall, both controllers behave similarly to each other for most of the target points within the workspace, demonstrating the effectiveness of both kinematic models within most of the workspace. However, the proposed differential kinematic model is superior in terms of the global stability near the workspace boundary. This is due to the fact that when the tip position of the continuum robot is close to the workspace boundary, the deviation between the actual shape of the robot and circular arc becomes nonnegligible. Therefore, model error will be imported into the kinematic model resulting from the conversion between arc parameters and tip position, resulting in the oscillation of the PCC-based controller in the neighbourhood of certain target point. On the contrary, the proposed controller is developed based on the novel differential kinematics, which abandons the arc parameters and thus avoids the conversion error.

b) Overall positioning performance

After the comparison with the PCC-based approach, a comprehensive set of tests were performed to characterize the overall positioning performance of the proposed controller.

As is shown in Fig. 8(a), the scanning path covering the whole workspace of the continuum robot was divided into four quadrants mainly owing to the measuring range and stability of the VICON system, which are marked using different colors (red, green, blue, and black). Fig. 8(b) gives the top view of the scanning paths, which are composed of discrete points whose projection in the XY plane are evenly distributed in the region $\Omega = \{(x, y) | \, x, y \in [-40,40]\}$ in the interval of $2.5mm$. And the time interval for updating the target point is 3.5s in the experiment.

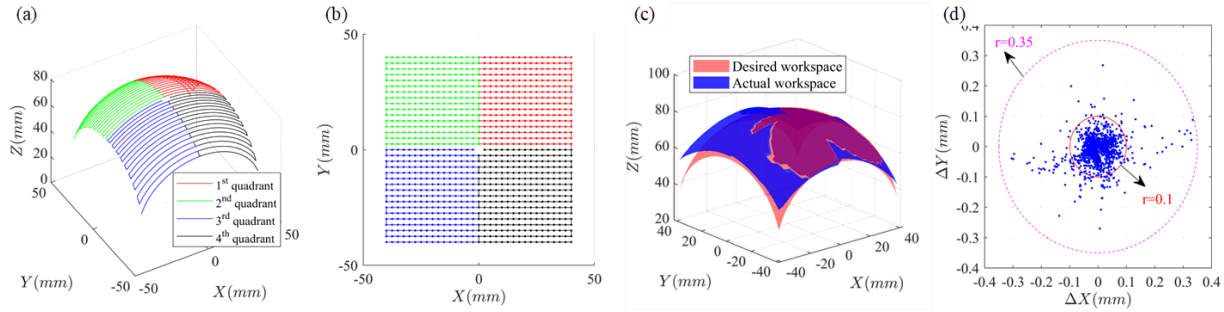

Fig. 8 Overall positioning performance of the proposed controller: (a) scanning path of tip position in 3D space; (b) top view of the scanning path with the tip position indicated by coloured dots; (c) desired workspace and actual workspace; (d) scatter diagram of the positioning error in X and Y axes for all 1088 test points. (This set of experiments was taken by VICON system. The static error of the system is $\pm 0.15 \pm 0.025mm$ [30].)

Fig. 8(c) compares the actual workspace with the theoretical workspace. It can be observed that there is a positive offset in the Z axis between the actual and theoretical workspaces, and the offset value becomes larger

as the bending angle increases. The factor contributing to this phenomenon is that all the disks are incompressible rigid bodies, which cannot deform elastically as the NiTi rods do to form an arc-like shape. While Fig. 8(d) shows the scatter diagram of the positioning error $(\Delta X, \Delta Y)$ for all target points. According to [30], the static error of the motion capture system used in this paper is 0.15mm. Which illustrates that the overall positioning accuracy is $\pm 0.35 \pm 0.15mm$ in the XY plane, and $\pm 0.18mm$ control accuracy can be reached for over 60% of the tested points.

3.3 Experiment II: path tracking

This section presents the experimental results of path tracking. First, comparisons are conducted between the PCC-based and the proposed controllers with the twin-pivot design. Then, the proposed controller is also implemented on the dual-revolute (Fig. 6(b)) and soft-robot (Fig. 6(c)) designs for comprehensive performance characterization.

The numerical comparisons of both controllers are given using RMSE (root mean square error) and maximum error as the performance indices. The RMSE of the PCC-based approach is slightly smaller than the proposed method, whose performance exceeds the former one in aspect of maximum error.

Two different spatial trajectories are used for the experiments of path tracking: the first path (Path I) is a segmented curve whose projection is a 20mm×20mm square centered at $(-15,15)$ in the XY plane while the second path (Path II) is a smooth curve whose projection is a 20mm-diameter circle centered at $(-15,15)$. Since both approaches are essentially static controllers, each path is discretized into a series of points, and the path tracking is achieved by updating the target position in a constant time interval (1s). In addition, both controllers are running at the frequency of 20 Hz, which is mainly restricted by the communication speed and execution time of the actuation system.

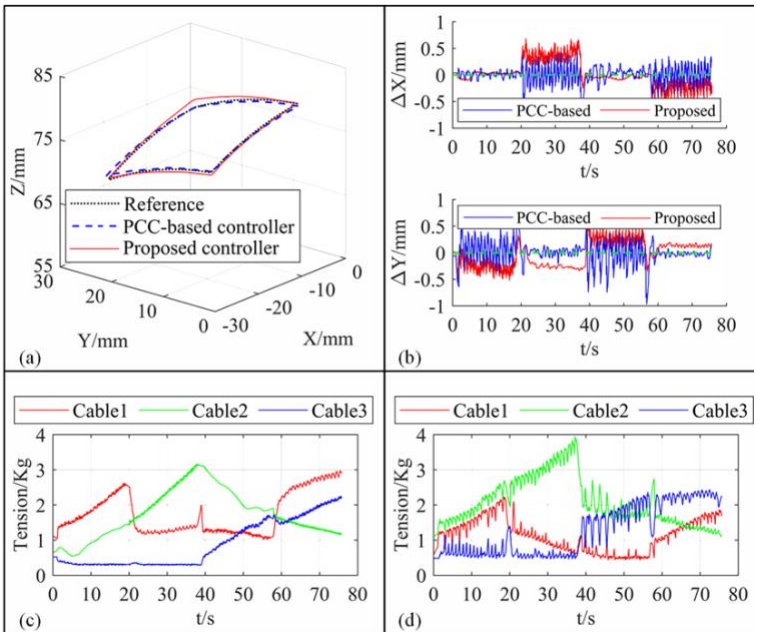

Fig. 9 Experimental comparison of both controllers tracking Path I: (a) desired trajectory (dotted line in black), actual trajectories based on the PCC-based controller (line in blue) and the proposed controller (dashed line in red); (b) positioning error in X and Y axes; (c) cable tensions with proposed controller; (d) cable tensions with PCC-based controller. (This set of experiments was taken by VICON system. The dynamic error of the system is 0.3mm [30].)

Fig.9 gives the experimental results of Path I. The desired path for reference and the actual trajectories obtained by the PCC-based and the proposed controllers are shown in Fig.9 (a). Also, the tracking errors $(\Delta X, \Delta Y)$ of both controllers in the X and Y axes are plotted in Fig.9 (b). Furthermore, the real-time changes of cable tensions are monitored for both controllers, which are given in Fig.9 (c) and (d), respectively. The fluctuations of cable tensions for the proposed controller are much smoother than the PCC-based controller. Likewise, the experimental results of Path II are illustrated in Fig. 10.

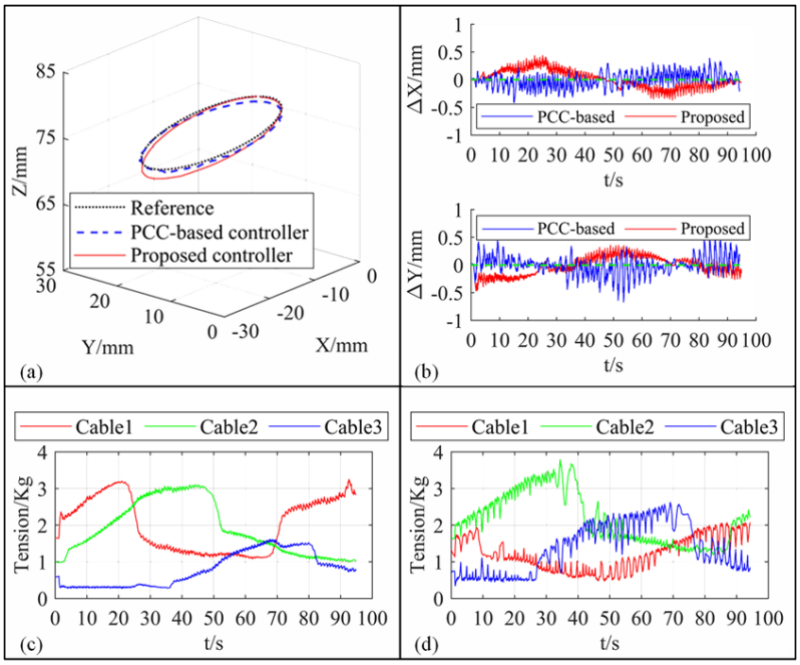

Fig. 10 Experimental comparison of both controllers tracking Path II: (a) desired trajectory (dotted line in black), actual trajectories based on the PCC-based controller (line in blue) and the proposed controller (dashed line in red); (b) positioning error in X and Y axes; (c) cable tensions with proposed controller; (d) cable tensions with PCC-based controller. (This set of experiments was taken by VICON system. The dynamic error of the system is 0.3mm [30].)

The numerical comparisons of both controllers are given in Table I, including RMSE (root mean square error) and maximum error. The RMSE of the PCC-based approach is slightly smaller than the proposed method, whose performance exceeds the former one in terms of maximum tracking error. Furthermore, as shown in Table II, the performance of the proposed controller has also been characterized on the dual-revolute and soft-robot designs.

Table I: Numerical comparison of both controllers on the twin-pivot design for path tracking

	Path I		**Path II**	
	RMSE	**Max error**	**RMSE**	**Max error**
PCC-based controller	0.17 mm	0.67 mm	0.21 mm	0.97 mm
Proposed controller	0.21 mm	0.47 mm	0.31 mm	0.72 mm

In order to demonstrate the robustness of the controller, we used one optimized design (twin-pivot design) (**Table I**) and two unoptimized designs (a dual-revolute design and a soft-robot design) to demonstrate the performance of the controller (**Table II**). It can be noted that the numerical performance of the three designs are incomparable due to the intrinsic issue of the dual-revolute based and soft continuum sections. Specifically, the dual-revolute design and the soft-robot design have a higher tracking error compared with the twin-pivot design. This is caused by the design of these two prototypes. For the dual-revolute design, the friction between the rigid joints is significant, which added an extra challenge for the controller. Similarly, the compression and the torsion of the soft section introduced more uncertainties for the control. Hence, the errors of these two designs are higher than the optimized twin-pivot design.

Table II: Path tracking performance of the dual-revolute and soft-robot designs with the proposed controller

	Path I		**Path II**	
	RMSE	**Max error**	**RMSE**	**Max error**
Dual-revolute design	0.7 mm	2.14 mm	1.04 mm	2.02 mm
Soft-robot design	0.4 mm	1.62 mm	0.53 mm	1.13 mm

In conclusion, the effectiveness of the novel proposed controller is experimentally validated on the twin-pivot, the dual-revolute and the soft-robot designs. Among the three prototypes, the best control performance (RMSE and max error) has been achieved on the twin-pivot design. Furthermore, strictly speaking, the proposed

controller is unsuitable for the soft robot, since the differential kinematics does not work if the backbone length variable S is not a constant. However, since the controllers are all developed for quasi-static control, together with the fact that the compression rate of the soft robot is quite low (under 6%, the maximum shrink length is around 5mm, and the original full length is 80mm), the backbone length can be approximated as constant in the short term of operation. Therefore, the proposed controller can still be applied on the soft robot, as demonstrated in the experiments.

4 Conclusion

This paper presents a novel model-based hybrid controller for the high-performance control of various single-section continuum robots, which has two main features: firstly, an analytical differential kinematic model , directly from task space to actuation space, is developed by describing the tip position in Cylindrical coordinate system instead of the Cartesian coordinate system and applying piecewise linear approximation. This avoids the explicit call of arc parameters. Secondly, based on the preliminary analysis of common control modes for tendon-driven continuum robots and combining the advantage of single-section continuum robots, a hybrid control scheme is proposed to decouple the control of cable displacements so that tension supervision can be achieved to avoid slack or over-tension states of driving cables.

Further, for evaluating the controllers, a set of experimental validation is carried out from two aspects, i.e., stability and versatility. On one hand, the proposed hybrid controller is compared with the PCC-based one on the twin-pivot-based continuum robot. It turns out that both controllers are mostly equivalent to each other, but the proposed controller outperforms the PCC-based one in terms of global stability for tip positioning and the tension fluctuations for path tracking. On the other hand, comprehensive experiments are conducted on three prototypes of continuum robots for the performance characterization of the proposed controller. The versatility of the proposed controller is demonstrated. Also, it can be found that the controller performs best on the twin-pivot design in aspects of RMSE (0.31 mm) and maximum deviation error (0.72 mm) for path tracking.

Future work will include extending hybrid control scheme for multi-section continuum robots and developing dynamic controller with the modified kinematic model. The combination of cable displacement/tension control can further be implemented to operate extra DoF of soft robots owing to the elasticity of the fabricating material. In addition, since the state space equation can be obtained based on the proposed differential kinematics, dynamic control can also be developed for smooth/continuous trajectory following.

Acknowledgment

The research leading to these results has received funding from Innovate UK under CHIMERA - Robotic Inspection of Pressure Vessels (104823), China Scholarship Council (CSC) and University of Nottingham.

References

[1] M. Russo *et al.*, "Continuum Robots: An Overview," *Advanced Intelligent Systems,* vol. 5, no. 5, p. 2200367, 2023, doi: https://doi.org/10.1002/aisy.202200367.

[2] S. Li and G. Hao, "Current Trends and Prospects in Compliant Continuum Robots: A Survey," *Actuators,* vol. 10, no. 7, p. 145, 2021. [Online]. Available: https://www.mdpi.com/2076-0825/10/7/145.

[3] M. C. Yip, J. A. Sganga, and D. B. Camarillo, "Autonomous control of continuum robot manipulators for complex cardiac ablation tasks," *Journal of Medical Robotics Research,* vol. 2, no. 01, p. 1750002, 2017.

[4] X. Dong *et al.*, "Development of a slender continuum robotic system for on-wing inspection/repair of gas turbine engines," *Robotics and Computer-Integrated Manufacturing,* vol. 44, pp. 218-229, 2017.

[5] M. Wang, D. Palmer, X. Dong, D. Alatorre, D. Axinte, and A. Norton, "Design and development of a slender dual-structure continuum robot for in-situ aeroengine repair," in *2018 IEEE/RSJ International Conference on Intelligent Robots and Systems (IROS)*, 2018: IEEE, pp. 5648-5653.

[6] O. Lakhal, A. Melingui, and R. Merzouki, "Hybrid approach for modeling and solving of kinematics of a compact bionic handling assistant manipulator," *IEEE/ASME Transactions on Mechatronics,* vol. 21, no. 3, pp. 1326-1335, 2015.

[7] I. A. Seleem, H. El-Hussieny, and H. Ishii, "Recent Developments of Actuation Mechanisms

for Continuum Robots: A Review," *International Journal of Control, Automation and Systems,* vol. 21, no. 5, pp. 1592-1609, 2023/05/01 2023, doi: 10.1007/s12555-022-0159-8.
[8] D. Baek, Y.-H. Nho, and D.-S. Kwon, "ViO-Com: Feed-Forward Compensation Using Vision-Based Optimization for High-Precision Surgical Manipulation," *IEEE Robotics and Automation Letters,* vol. 7, no. 1, pp. 263-270, 2021.
[9] D. Nguyen *et al.*, "A Hybrid Concentric Tube Robot for Cholesteatoma Laser Surgery," *IEEE Robotics and Automation Letters,* vol. 7, no. 1, pp. 462-469, 2021.
[10] S. Satheeshbabu, N. K. Uppalapati, G. Chowdhary, and G. Krishnan, "Open Loop Position Control of Soft Continuum Arm Using Deep Reinforcement Learning," in *2019 International Conference on Robotics and Automation (ICRA)*, 2019: IEEE, pp. 5133-5139.
[11] M. Giorelli, F. Renda, M. Calisti, A. Arienti, G. Ferri, and C. Laschi, "Neural network and jacobian method for solving the inverse statics of a cable-driven soft arm with nonconstant curvature," *IEEE Transactions on Robotics,* vol. 31, no. 4, pp. 823-834, 2015.
[12] B. A. Jones and I. D. Walker, "Practical kinematics for real-time implementation of continuum robots," *IEEE Transactions on Robotics,* vol. 22, no. 6, pp. 1087-1099, 2006.
[13] R. J. Webster III and B. A. Jones, "Design and kinematic modeling of constant curvature continuum robots: A review," *The International Journal of Robotics Research,* vol. 29, no. 13, pp. 1661-1683, 2010.
[14] C. Escande, T. Chettibi, R. Merzouki, V. Coelen, and P. M. Pathak, "Kinematic calibration of a multisection bionic manipulator," *IEEE/ASME transactions on mechatronics,* vol. 20, no. 2, pp. 663-674, 2015.
[15] M. Li, R. Kang, S. Geng, and E. Guglielmino, "Design and control of a tendon-driven continuum robot," *Transactions of the Institute of Measurement and Control,* vol. 40, no. 11, pp. 3263-3272, 2018.
[16] Y. Bailly, Y. Amirat, and G. Fried, "Modeling and control of a continuum style microrobot for endovascular surgery," *IEEE Transactions on Robotics,* vol. 27, no. 5, pp. 1024-1030, 2011.
[17] P. Qi, C. Liu, A. Ataka, H.-K. Lam, and K. Althoefer, "Kinematic control of continuum manipulators using a fuzzy-model-based approach," *IEEE Transactions on Industrial Electronics,* vol. 63, no. 8, pp. 5022-5035, 2016.
[18] R. S. Penning, J. Jung, J. A. Borgstadt, N. J. Ferrier, and M. R. Zinn, "Towards closed loop control of a continuum robotic manipulator for medical applications," in *Robotics and Automation (ICRA), 2011 IEEE International Conference on*, 2011: IEEE, pp. 4822-4827.
[19] M. C. Yip and D. B. Camarillo, "Model-less feedback control of continuum manipulators in constrained environments," *IEEE Transactions on Robotics,* vol. 30, no. 4, pp. 880-889, 2014.
[20] Y. Jin *et al.*, "Model-less feedback control for soft manipulators," in *Intelligent Robots and Systems (IROS), 2017 IEEE/RSJ International Conference on*, 2017: IEEE, pp. 2916-2922.
[21] K.-H. Lee *et al.*, "Nonparametric Online Learning Control for Soft Continuum Robot: An Enabling Technique for Effective Endoscopic Navigation," *Soft robotics,* vol. 4, no. 4, pp. 324-337, 2017.
[22] M. Li, R. Kang, D. T. Branson, and J. S. Dai, "Model-free control for continuum robots based on an adaptive Kalman filter," *IEEE/ASME Trans. Mechatron,* vol. 23, no. 1, pp. 286-297, 2018.
[23] A. Melingui, O. Lakhal, B. Daachi, J. B. Mbede, and R. Merzouki, "Adaptive neural network control of a compact bionic handling arm," *IEEE/ASME Transactions on Mechatronics,* vol. 20, no. 6, pp. 2862-2875, 2015.
[24] T. George Thuruthel, E. Falotico, M. Manti, A. Pratesi, M. Cianchetti, and C. Laschi, "Learning closed loop kinematic controllers for continuum manipulators in unstructured environments," *Soft robotics,* vol. 4, no. 3, pp. 285-296, 2017.
[25] X. Li, J. Zhang, J. Zhao, G. Zhang, and C. Shi, "A Model-Free Method-Based Shape Reconstruction for Cable-Driven Continuum Manipulator Using Artificial Neural Network,"

in *2019 IEEE International Conference on Robotics and Biomimetics (ROBIO)*, 6-8 Dec. 2019 2019, pp. 1424-1429, doi: 10.1109/ROBIO49542.2019.8961822.

[26] T. George Thuruthel, Y. Ansari, E. Falotico, and C. Laschi, "Control Strategies for Soft Robotic Manipulators: A Survey," *Soft Robotics,* vol. 5, no. 2, pp. 149-163, 2018/04/01 2018, doi: 10.1089/soro.2017.0007.

[27] X. Dong, M. Raffles, S. Cobos-Guzman, D. Axinte, and J. Kell, "A novel continuum robot using twin-pivot compliant joints: design, modeling, and validation," *Journal of Mechanisms and Robotics,* vol. 8, no. 2, p. 021010, 2016.

[28] W. Ba, X. Dong, A. Mohammad, M. Wang, D. Axinte, and A. Norton, "Design and validation of a novel fuzzy-logic-based static feedback controller for tendon-driven continuum robots," *IEEE/ASME Transactions on Mechatronics,* 2021.

[29] R. S. Penning, J. Jung, N. J. Ferrier, and M. R. Zinn, "An evaluation of closed-loop control options for continuum manipulators," in *2012 IEEE International Conference on Robotics and Automation*, 2012: IEEE, pp. 5392-5397.

[30] P. Merriaux, Y. Dupuis, R. Boutteau, P. Vasseur, and X. Savatier, "A Study of Vicon System Positioning Performance," *Sensors*, vol. 17, no. 7, doi: 10.3390/s17071591.